atmosphere

MDPI

Article

Spatial Variability of Glaciochemistry along a Transect from Zhongshan Station to LGB69, Antarctica

Weilong Huang [1,2], Ming Yan [1,*], Robert Mulvaney [3], Zuoqin Qian [2], Leibao Liu [1], Chunlei An [1], Cunde Xiao [4] and Yujia Zhang [2]

1 Key Laboratory of Polar Science, MNR, Polar Research Institute of China, Shanghai 200136, China; hwl220@whut.edu.cn (W.H.); liuleibao@pric.org.cn (L.L.); anchunlei@pric.org.cn (C.A.)
2 School of Energy and Power Engineering, Wuhan University of Technology, Wuhan 430063, China; qzq@whut.edu.cn (Z.Q.); zhangyujia@whut.edu.cn (Y.Z.)
3 British Antarctic Survey, High Cross, Madingley Road, Cambridge CB3 0ET, UK; rmu@bas.ac.uk
4 State Key Laboratory of Land Surface Processes and Resource Ecology, Beijing Normal University, Beijing 100875, China; cdxiao@lzb.ac.cn
* Correspondence: mingyan@pric.org.cn; Tel.: +86-21-5871-3652

Abstract: The spatial glaciochemical variability of snow samples collected along a transect from Zhongshan Station to Lambert Glacier Basin 69 (LGB69) in Antarctica was investigated. Sea-salt ion concentrations exponentially decreased with increasing distance from the coast and/or altitude. The observed high sea-salt ion concentrations within 20.6 km of the coast may be related to preferential wet or dry deposition of sea-salt aerosols. Methanesulfonic acid (MSA), non-sea-salt sulfate ($nssSO_4^{2-}$), and calcium (Ca^{2+}) concentrations decreased along the transect. The mean MSA/$nssSO_4^{2-}$ value of the surface snow samples (0.34 ± 0.08) indicates that coastal sea areas are their likely source regions. The non-sea-salt Ca^{2+} ($nssCa^{2+}$)/Ca^{2+} percentages of the surface snow and LGB69 snow pit samples reveal that continental dust is the primary Ca^{2+} source. The δD and $\delta^{18}O$ values decreased from the coast inland. The variation of deuterium excess (d-excess) along the transect was stable and d-excess values in the two snow pit samples were low and similar, which indicates that the moisture source region between Zhongshan Station and LGB69 is a coastal sea area. These results reveal the spatial distribution patterns and sources of ions and stable isotopes, as well as factors that influence the deposition of ions and the composition of stable isotopes, which provide important insight for further studies of ice cores drilled in Antarctic coastal regions.

Keywords: ionic composition; stable isotope; spatial variability; Antarctica

check for updates

Citation: Huang, W.; Yan, M.; Mulvaney, R.; Qian, Z.; Liu, L.; An, C.; Xiao, C.; Zhang, Y. Spatial Variability of Glaciochemistry along a Transect from Zhongshan Station to LGB69, Antarctica. *Atmosphere* **2021**, *12*, 393. https://doi.org/10.3390/atmos12030393

Academic Editor: Renato R. Colucci

Received: 20 January 2021
Accepted: 12 March 2021
Published: 17 March 2021

Publisher's Note: MDPI stays neutral with regard to jurisdictional claims in published maps and institutional affiliations.

Copyright: © 2021 by the authors. Licensee MDPI, Basel, Switzerland. This article is an open access article distributed under the terms and conditions of the Creative Commons Attribution (CC BY) license (https://creativecommons.org/licenses/by/4.0/).

1. Introduction

The ionic and isotopic compositions of Antarctic snow can serve as important indicators of environmental and climatic information [1]. These indicators include sea-salt ions, sulfur components, and stable isotopes. Sea-salt ions (mainly Cl^-, Na^+, and Mg^{2+}) come from sea ice and/or sea water [2,3], which are strongly influenced by sea-ice extent and meteorological conditions [4,5]. Marine sulfur components (non-sea-salt sulfate ($nssSO_4^{2-}$) and methanesulfonic acid (MSA)) can be attributed to marine biogenic activity via dimethyl sulfide (DMS) oxidation [6]. DMS is the only source of MSA, and thus MSA is the best alternative indicator for DMS [7–9]. In contrast, $nssSO_4^{2-}$ has various sources, such as volcanic eruptions, anthropogenic emissions, and crustal erosion [10]. The $nssSO_4^{2-}$ from volcanic eruptions can be used to date ice cores [10,11] based on the eruption history [12–14]. Stable isotopes (δD and $\delta^{18}O$) reflect climate variations over time and space and are commonly used to quantify changes of air temperature in past environments. Deuterium excess (d-excess) is a second-order parameter used to identify moisture source regions [15–17].

High-resolution climate records are often obtained from ice cores drilled at sites with high annual accumulation rates. These data are used to interpret temporal variations

of chemical ions and isotopes on different scales and can reveal important information regarding past oceanic and atmospheric environment changes [18–20]. To comprehensively interpret the temporal variations of chemical ions and isotopes from ice cores drilled at a given site, it is necessary to understand the spatial distribution patterns, sources, and factors that influence the deposition of chemical components in the snow in the same region [21].

The Chinese National Antarctic Research Expedition (CHINARE) involved travel inland along a transect from Zhongshan Station to Dome A [11,22–28] (Figure 1). The spatial variability of ions in snow samples from Zhongshan station to Dome A has been systematically studied. These results suggested that sea-salt ion concentrations decreased with increasing distance from the coast and altitude, and that the spatial variations are related to different sources, transport, and depositional processes. Similar trends of sea-salt ions were also observed in other transects from the Antarctic coast inland [21,29–31]. Cl^-/Na^+ ratios increased with increasing distance from the coast and altitude owing to other Cl^- sources and post-depositional effects in the interior region of the transect. The $MSA/nssSO_4^{2-}$ ratio in coastal areas was higher than that in inland areas because of different source regions and transport pathways [27,28].

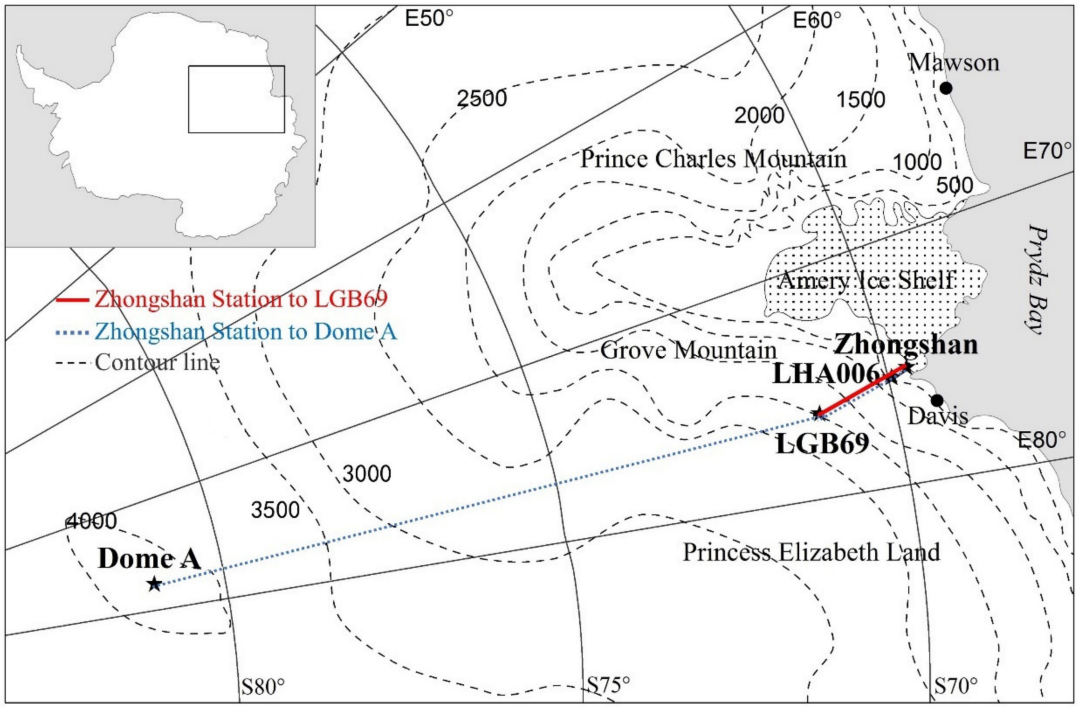

Figure 1. Sampling location. The red line indicates the transect from Zhongshan Station to LGB69 in this study; The blue dash indicates the entire transect from Zhongshan Station to Dome A; The black dash indicates contour line.

Previous investigations of stable isotopes from surface snow samples along the transect from Zhongshan Station to Dome A showed that δD and $\delta^{18}O$ values negatively correlated with distance from the coast and altitude and that the $\delta D/\delta^{18}O$ ratio was lower than that of the Global Meteoric Water Line (GMWL) and the mean value for Antarctica (7.75) [24,26]. This implies that more intense kinetic fractionation processes occur during snow formation in the interior region of the transect [26,27]. Previous studies indicated a significant increase of Antarctic d-excess values at altitudes near or above 2000 m owing to different moisture origins [15,32]. The d-excess values along the transect from Zhongshan Station to Dome A exhibited a positive trend in the inland direction, with a step change as a function of either distance to the coast or latitude characterized by higher values for elevations above ~2750 m. It has been speculated that a specific transport path brings moisture toward Dome A either from warm, distant moisture sources, or from sea-ice edge areas [17,26,27].

Ding et al. [33] showed that the coastal region (68–202 km) of the transect from Zhongshan Station to Dome A is characterized by a relatively high average annual accumulation rate (157 kg m^{-2} a^{-1}), which indicates the ice cores drilled in the coastal region of the transect can provide high-resolution chemical ion and isotope records [34]. Moreover, the transect from Zhongshan Station to Dome A covers a distance of 1256 km and a wide range of environments. Different regions of the transect have diverse environments (e.g., the coast region has high accumulation rate, whereas very low accumulation rate is observed in the inland region [33]), which cause various distribution characteristics of chemical components [27]. Thus, it is necessary to collect more data and study each region individually. At present, some investigations have been carried out to reveal the spatial patterns of ions and stable isotopes along the entire transect from Zhongshan Station to Dome A [24,26,27]. However, due to limited snow chemistry data of coastal region in the past, there have only been a few systematic studies on the spatial distribution, sources, and factors that influence the deposition of the chemical components in the coastal region of the transect from Zhongshan Station to Dome A [24,26,27].

In this study, the spatial variability of the ionic and isotopic compositions of samples from surface snow and two snow pits obtained along a transect from Zhongshan Station to LGB69 was analyzed. In particular, surface snow and snow pit samples were collected in the steep coastal escarpment region within 20.6 km distance from Zhongshan Station, which were less documented in previous research [24,26,27]. The results provide a detailed illustration of the spatial distribution patterns and sources of the ions and stable isotopes, as well as factors that influence the deposition of ions and the composition of stable isotopes. This study not only fills in a gap of snow chemistry investigation within 20.6 km distance from the coast along the transect from Zhongshan Station to Dome A, but also contributes to the interpretation of long-term chemical records obtained from ice cores drilled in the coastal regions of Princess Elizabeth Land.

2. Sampling and Laboratory Analysis

2.1. Sample Collection

Seventeen surface snow samples and two snow pit samples were collected along the transect from Zhongshan Station to LGB69 during the austral summer of the 18th CHINARE (2001–2002) (Figure 1). The end site LGB69 is located at 70°50′06″ S and 77°04′29″ E in Princess Elizabeth Land of East Antarctica, approximately 172 km (route distance) from Zhongshan Station, at an altitude of 1860 m. The annual accumulation rate at LGB69 is as high as 255 kg m^{-2} a^{-1} based on snow pit dating and water equivalent depth. The transect from Zhongshan Station to LGB69 shows a clear difference in altitude changes between the coast and the inland region. Within 20.6 km (distance from the coast, unless otherwise mentioned), the altitude increases rapidly from 0 to 586 m, indicating a steep coastal escarpment region. Beyond 20.6 km, the altitude rises gradually from 586 to 1852 m (Table 1). The slope was calculated as the altitude change/distance change between the two sites. Figure 2 shows the slope variation from the coast inland, as listed in Table 1. The steep coastal escarpment region within 20.6 km has an average slope of 28.4 m km^{-1}, whereas the interior region between 20.6 and 170 km has an average slope of 8.4 m km^{-1}.

Surface snow samples were collected at approximately 10-km intervals along the transect from Zhongshan Station to LGB69. One surface snow sample was collected at each site. In total, 17 surface snow samples were obtained to analyze the spatial variability of their ionic and isotopic compositions. Table 1 provides the geographical information of the surface snow samples.

Two sites were selected for the snow pit sampling: LHA006 near the coast and LGB69 located inland. The snow pit samples were collected at 2-cm intervals to determine their ionic and isotopic compositions. Samples from two snow pits were also collected to assess the spatial variability of their ionic and isotopic compositions. Table 2 lists the geographical and sampling information of the two snow pits.

Table 1. Geographical information of the surface snow samples.

Site	Location	Slope (m km^{-1})	Altitude (m)	Route Distance from Zhongshan Station (km)
LH9601	69° 26′ 01″ S 76° 20′ 00″ E	38.5	285	7.4
LHA006	69°31′13.6″ S 76° 17′ 36″ E	22.4	520	17.9
L156	69° 33′ 57.2″ S 76° 16′ 05.7″ E	24.4	586	20.6
LH404	69° 36′ 32″ S 76° 25′ 15.3″ E	13.9	737	31.5
LH397	69° 42′37.3″ S 76° 28′ 29.6″ E	9.0	849	44.0
LH386	69° 48′ 30.8″ S 76° 28′ 41.7″ E	9.5	955	55.2
LGB72	69° 55′ 16.9″ S 76° 29′ 22.7″ E	6.7	1041	68.0
LT987	70° 00′ 31.5″ S 76° 32′ 03.5″ E	11.6	1157	78.0
LT981	70° 06′ 52″ S 76° 35′ 33″ E	11.1	1290	90.0
LT976	70° 12′ 00.6″ S 76° 38′ 14″ E	5.3	1343	100.0
LT971	70° 17′ 29.3″ S 76° 41′ 57″ E	7.4	1417	110.0
LT966	70° 22′ 52″ S 76° 45′ 11″ E	10.3	1520	120.0
LT961	70° 28′ 07″ S 76° 47′ 51.5″ E	4.5	1565	130.0
LT956	70° 33′23.4″ S 76° 51′ 15.2″ E	9.2	1657	140.0
LT951	70° 38′ 37.7″ S 76° 55′ 24″ E	7.2	1729	150.0
LT946	70° 43′ 48.8″ S 76° 59′ 36.5″ E	5.7	1786	160.0
LT941	70° 49′ 02″ S 77° 03′ 40.6″ E	6.6	1852	170.0

Table 2. Geographical and sampling information of the two snow pits.

Site	LHA006	LGB69
Depth (m)	1.0	1.8
Sample number	50	90
Altitude (m)	520	1860
Slope (m km^{-1})	22.4	4.0
Distance from the coast (km)	17.9	172
Annual accumulation rate * (kg m^{-2} a^{-1})	200	255

* Calculation of the accumulation rate based on snow pit dating and water equivalent depths.

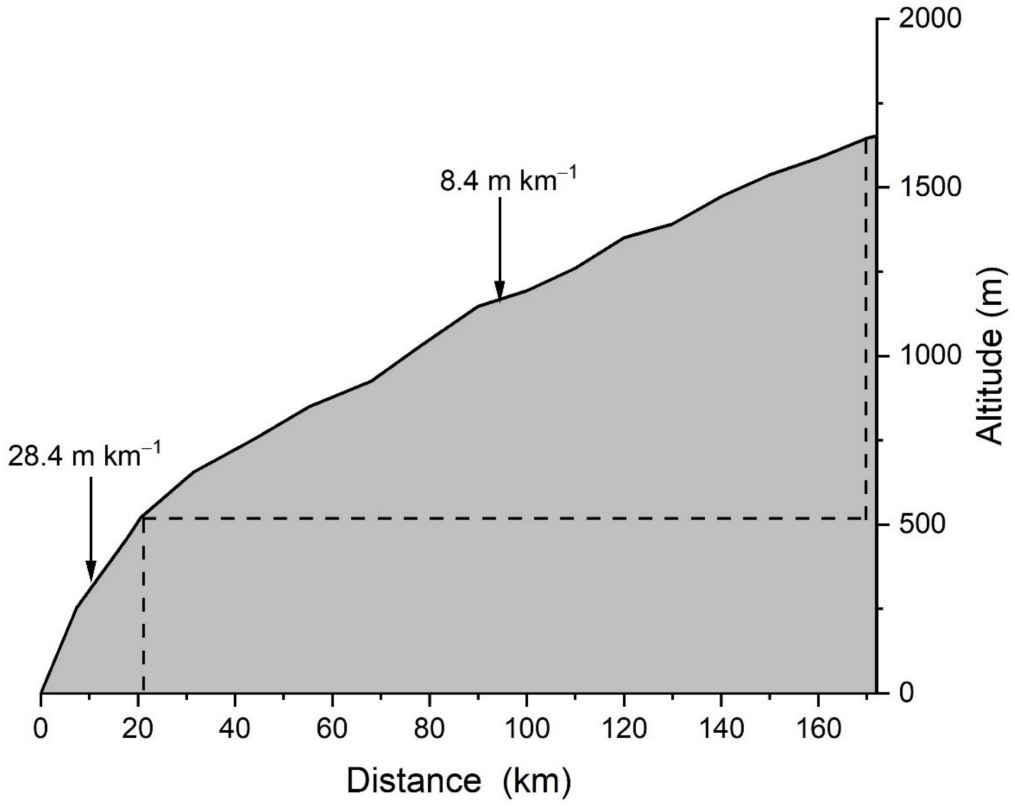

Figure 2. Slope variation along the transect.

2.2. Sample Analysis

The chemical samples were measured in the 100-class clean laboratory of the British Antarctic Survey. Anions and cations were analyzed simultaneously and a selection of chemical concentrations (F^-, Cl^-, NO_3^-, SO_4^{2-}, MSA, Na^+, K^+, Ca^{2+}, and Mg^{2+}) was obtained using two Dionex ion chromatographs (DX 500, Autosampler, Chromeleon 6.6 chromatograph data system). Strict anti-contamination measures were adopted during the entire process of sample cutting, melting, and analysis. 18.2 MΩ·cm ELGA UHP water was used to clean the sample processing equipment and containers and to prepare blank samples and working standards. Analytical columns (AS18 and CS12A) and guard columns (AG18 and CG12A) were respectively used in the anion and cation measurements using an injection volume of 200 µL. The eluent conditions were chosen to result in similar run length of 12 min for both cations and anions, to allow simultaneous injection from the same autosampler vial. For the anions, isocratic elution used a 20 mM potassium hydroxide eluent at a flow rate of 1.0 mL per minute, while the cations were eluted isochratically with 20 mM methane sulphonic acid eluent at a flow rate of 1.0 mL per minute. Five multi-ion standards were prepared to bracket the range of concentrations measured in the traverse samples. The blank samples were regularly monitored during the analysis and the main chemical components of all blank samples were lower than the detection limit.

The stable isotope samples were measured on the liquid water isotope analyzer (DLT-100, Los Gatos Research, Inc., Mountain View, CA, USA) at the British Antarctic Survey. Hydrogen and oxygen isotopes were simultaneously analyzed. The DLT-100 was calibrated using working standards that bracketed the transect samples which had been prepared and calibrated against primary V-SMOW (Vienna Standard Mean Ocean Water) and V-SLAP (Vienna Standard Antarctic Precipitation) standards by the NERC Isotope Geosciences Laboratory (Keyworth, UK) using an Isoprime Isotope Ratio Mass Spectrometer. The accuracy of the δD or $\delta^{18}O$ analysis (±0.8‰ and ±0.1‰, respectively) is comparable to that of traditional stable isotope mass spectrometry [35]. Some comparison samples were

measured on the Isoprime mass spectrometers and the results are in good agreement with those obtained using the DLT-100.

3. Results and Discussion

3.1. Spatial Variability of Ionic Compositions

3.1.1. Sea-Salt Ions

The concentrations of Cl^-, Na^+, and Mg^{2+} were high in the surface snow samples, ranging from 952.48 to 1659.08, 970.78 to 1480.13, and 46.22 to 76.56 μg L^{-1}, respectively, between 7.4 and 20.6 km (285–586 m altitude). However, these concentrations exponentially decreased with increasing distance from the coast and altitude. The relatively low concentrations of Cl^-, Na^+, and Mg^{2+} (ranged from 14.67 to 184.64, 7.93 to 150.00, and 1.37 to 22.05 μg L^{-1}, respectively) were observed between 31.5 and 170 km (737–1852 m altitude) (Figure 3). The detailed Cl^-, Na^+, and Mg^{2+} concentrations of the surface snow samples along the transect from Zhongshan Station to LGB69 are shown in Table 3. Moreover, because of significant correlation between distance from coast and altitude (R = 0.991, p <0.01), the variation trends of ions and stable isotopes with altitude are similar to those with distance from coast and not shown in the figures.

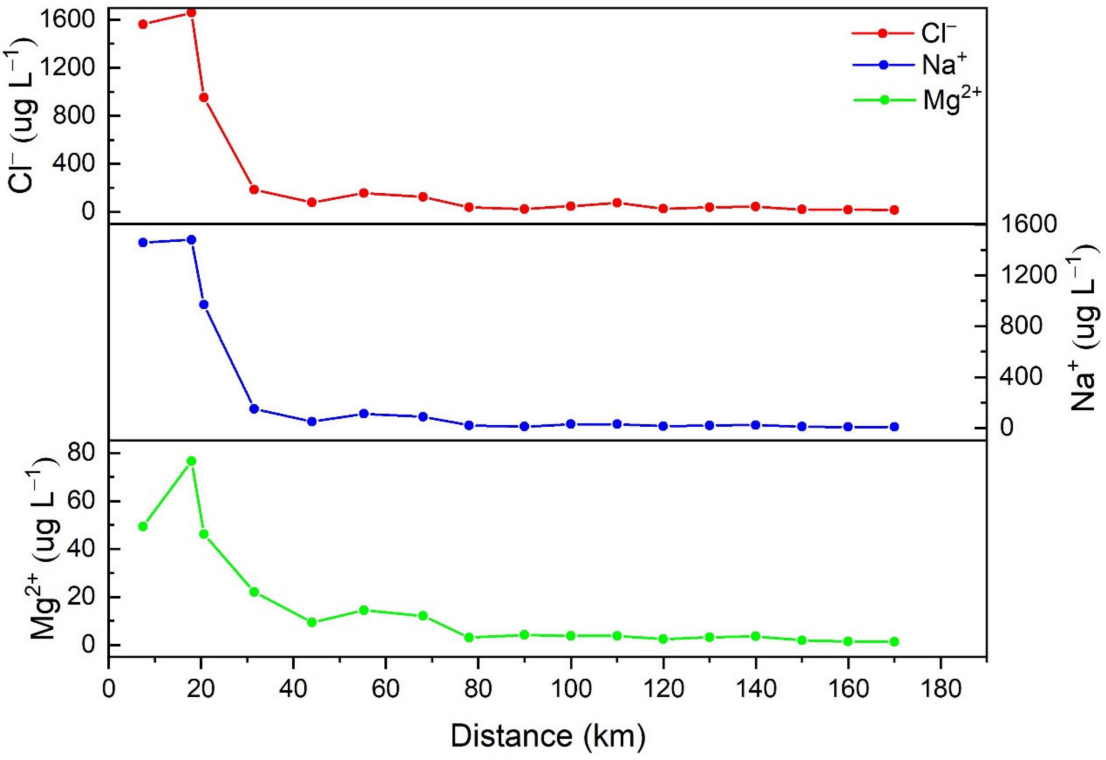

Figure 3. Concentration variations of Cl^-, Na^+, and Mg^{2+} with increasing distance from the coast. Each point represents the value of one surface snow sample for each site, unless otherwise mentioned.

High Cl^-, Na^+, and Mg^{2+} concentrations occurred specifically in the steep coastal escarpment region within 20.6 km (Figure 3). This may be related to the preferential wet or dry deposition of sea-salt aerosols. Sea-salt aerosols can be scavenged from the atmosphere by wet or dry deposition depending on the meteorological conditions. Most sea-salt aerosols can be deposited by snow precipitation in regions with high annual accumulation rates. High relative humidity conditions (60–70%) are conducive to the wet deposition of sea-salt aerosols [36]. In the present study, high accumulation rates and high relative humidity conditions (>60%) exist in the steep coastal escarpment region [33,37], leading to the preferential wet deposition of sea-salt aerosols. Alternatively, when local meteorological conditions are inadequate for wet deposition, the steep faces of the coastal

escarpment can intercept the maritime air mass with abundant sea-salt aerosols. Katabatic winds are highly unidirectional and persistent and prevail in the steep coastal escarpment regions of Antarctica [37–39]. The intercepted maritime air masses interact strongly with the katabatic winds over the steep coastal escarpments, which leads to turbulence, thereby inducing the dry deposition of sea-salt aerosols [36]. Consequently, high Cl^-, Na^+, and Mg^{2+} concentrations were found specifically in the steep coastal escarpment region within 20.6 km, which may be because of the preferential wet or dry deposition of sea-salt aerosols.

Table 3. Concentrations of major ions and values of stable isotopes of the surface snow samples from coast to inland.

Site	Na^+	Mg^{2+}	Ca^{2+}	Cl^-	MSA	SO_4^{2-}	$nssSO_4^{2-}$	$nssCa^{2+}$	δD	$\delta^{18}O$	d-Excess
					μg L^{-1}					‰	
LH9601	1458.92	49.32	27.63	1561.71	2.77	132.44	−235.93	−27.81	−123.57	−16.03	4.70
LHA006	1480.13	76.56	29.42	1659.08	143.02	399.60	25.86	−26.83	−83.82	−10.64	1.27
L156	970.78	46.22	12.17	952.48	112.22	347.64	102.52	−24.72	−111.84	−14.46	3.86
LH404	150.00	22.05	7.85	184.64	108.93	260.93	223.06	2.15	−128.96	−16.43	2.47
LH397	49.25	9.40	26.99	77.99	42.89	130.89	118.45	25.12	−144.86	−18.46	2.78
LH386	111.62	14.48	53.40	155.51	145.82	363.56	335.38	49.16	−139.09	−16.83	−4.47
LGB72	88.34	12.07	7.37	125.56	108.09	340.76	318.46	4.02	−154.95	−18.99	−3.01
LT987	20.37	3.07	6.93	37.34	24.89	93.79	88.65	6.16	−163.55	−20.53	0.73
LT981	10.88	4.16	3.66	23.85	17.67	80.87	78.12	3.25	−164.42	−20.91	2.83
LT976	29.35	3.77	11.51	47.71	40.92	169.65	162.24	10.40	−174.39	−22.00	1.64
LT971	29.27	3.82	14.76	75.36	42.51	161.71	154.31	13.64	−169.00	−21.58	3.63
LT966	14.81	2.44	2.37	25.08	20.93	62.22	58.48	1.81	−168.83	−21.73	4.97
LT961	19.51	3.22	2.01	38.72	44.25	122.28	117.35	1.27	−180.78	−22.70	0.78
LT956	23.05	3.59	2.04	42.50	48.09	110.53	104.71	1.17	−183.75	−23.27	2.44
LT951	10.98	1.89	3.85	19.36	29.16	93.99	91.22	3.44	−184.92	−23.32	1.66
LT946	7.93	1.40	2.83	17.80	31.21	78.79	76.79	2.53	−193.52	−24.76	4.53
LT941	8.13	1.37	1.44	14.67	17.60	72.49	70.43	1.14	−193.06	−24.39	2.04

Cl^-, Na^+, and Mg^{2+} were also typically strongly positively correlated with one another (Table 4), which indicates they are from the same source. The sea-salt ions exhibited significant negative correlations with distance from the coast or altitude (Table 4), suggesting that the spatial distributions of sea-salt ions from Zhongshan Station to LGB69 are mainly affected by distance from the coast and/or altitude.

Table 4. Correlation matrix of the major ions and $\delta^{18}O$ values of surface snow samples along with distance from the coast and altitude.

	Na^+	Mg^{2+}	Ca^{2+}	Cl^-	MSA	$nssSO_4^{2-}$	$\delta^{18}O$	Distance	Altitude
Na^+	1	0.959 *	0.427	0.998 *	0.309	−0.576 †	0.789 *	−0.692 *	−0.768 *
Mg^{2+}		1	0.480	0.963 *	0.530 †	−0.370	0.900 *	−0.762 *	−0.813 *
Ca^{2+}			1	0.446	0.533 †	0.106	0.639 *	−0.620 *	−0.619 *
Cl^-				1	0.320	−0.567 †	0.796 *	−0.693 *	−0.768 *
MSA					1	0.574 †	0.699 *	−0.533†	−0.493†
$nssSO_4^{2-}$						1	−0.067	0.089	0.188
$\delta^{18}O$							1	−0.929 *	−0.929 *
Distance								1	0.991 *
Altitude									1

* Data are significantly correlated at $p < 0.01$; † Data are significantly correlated at $p < 0.05$.

Cl^-/Na^+ ratios in the surface snow samples have been used to determine the effects of sources or post-depositional processes on the deposition of sea-salt components [5,40]. In the present study, Cl^-/Na^+ ratios were calculated from all of the surface snow samples, yielding an average ratio of 1.67 ± 0.44 from Zhongshan Station to LGB69, which was close to the ratio of sea water (1.81, W/W [41]). This suggests that sea salt is the main source of

Cl^- and Na^+ along the transect. Figure 4 shows the variation of Cl^-/Na^+ ratios from the coast inland. However, a few low Cl^-/Na^+ ratios occurred in the steep coastal escarpment region within 20.6 km. The lowest Cl^-/Na^+ ratio (0.98) was recorded at site L156 at 20.6 km (586 m altitude), followed by 1.07 from site LH9601 at 7.4 km (285 m altitude), and the average of Cl^-/Na^+ ratios was 1.06 ± 0.07 between 7.4 and 20.6 km. Beyond 20.6 km, the Cl^-/Na^+ ratios ranged from 1.23 to 2.57 with an average of 1.80 ± 0.36, which was almost equal to that of the sea water ratio (Table 5). Previous studies at coastal Antarctic sites suggested that at relatively low accumulation rates (<40 kg m^{-2} a^{-1}), the post-depositional loss of HCl becomes significant and reduces the Cl^- concentrations in snow, resulting in a reduced Cl^-/Na^+ ratio [5,42]. However, the present study region is characterized by a relatively high average snow accumulation rate (157 kg m^{-2} a^{-1}) [33]. For example, the Cl^-/Na^+ ratio of LHA006 at 17.9 km was only 1.12 (Table 5), whereas its annual accumulation rate reached as high as 200 kg m^{-2} a^{-1} (Table 2). The post-depositional loss of HCl can therefore not account for the low Cl^-/Na^+ ratios at these sites. Alternatively, Cl^- depletion may also be related to the reaction of sea-salt aerosols (mainly NaCl) with atmospheric acids (mainly HNO_3 and H_2SO_4). This reaction leads to the formation of gas-phase HCl, which lowers the initial Cl^-/Na^+ ratios of sea-salt aerosols [5,42]. However, there was no low Cl^-/Na^+ ratio occurred beyond 20.6 km. Thus, the reaction between sea-salt aerosols and atmospheric acids cannot be used to explain the low Cl^-/Na^+ ratios that only occurred in the steep coastal escarpment region within 20.6 km.

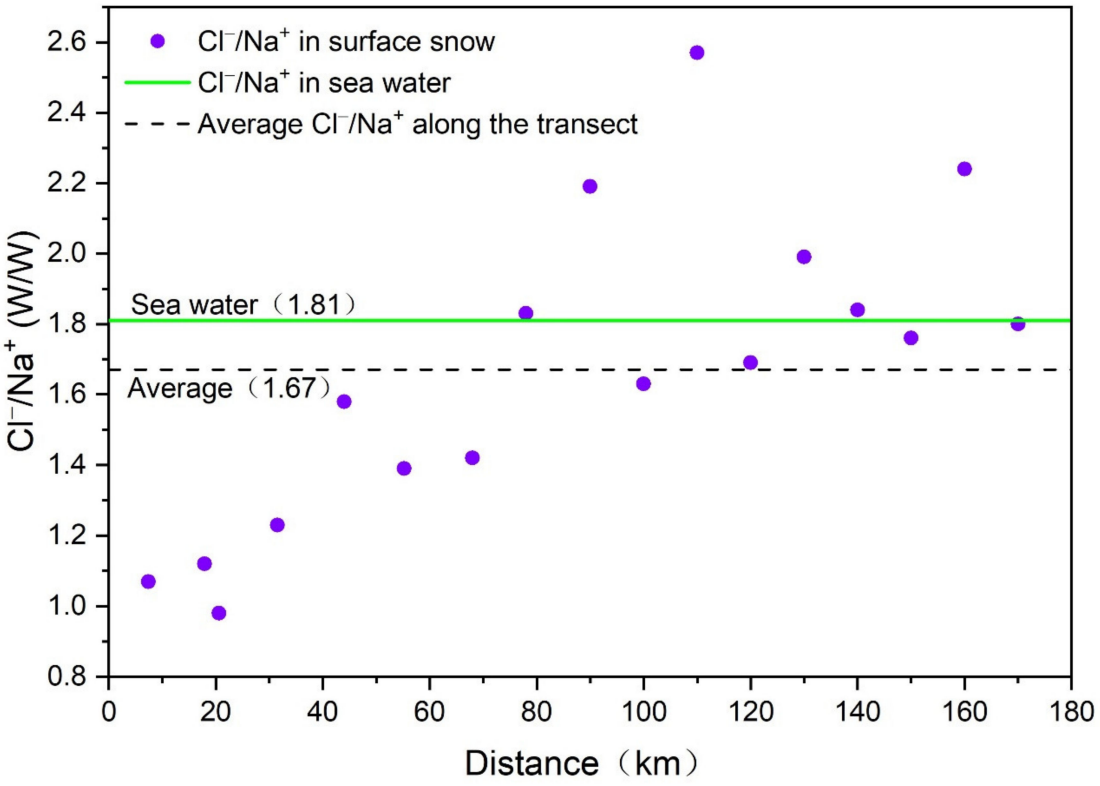

Figure 4. Variation of Cl^-/Na^+ ratios in the surface snow samples from the coast inland.

In the present surface snow samples, the observed low Cl^-/Na^+ ratios within 20.6 km may be related to the steep slopes of the coastal escarpment. The variations of surface slope of the Antarctic ice sheet have a strong impact on the wind speed and direction [43]. The steep slopes of the coastal escarpment can lead to wind redistribution, inducing snow redistribution. In the process of snow redistribution by wind scouring, the Na^+ concentrations can be increased by the continuous input of sea-salt aerosols. However, unlike Na^+, Cl^- is depleted owing to the reaction between sea-salt aerosols and atmospheric acids

during wind redistribution. The steep slopes of the coastal escarpment thus result in wind redistribution-induced snow redistribution, leading to an increase of Na^+ concentrations, thereby lowering the Cl^-/Na^+ ratios [36]. Consequently, the low Cl^-/Na^+ ratios within 20.6 km can be attributed to the steep slopes of the coastal escarpment.

Table 5. Detailed values of Cl^-/Na^+, $nssSO_4^{2-}/SO_4^{2-}$, $MSA/nssSO_4^{2-}$, and $nssCa^{2+}/Ca^{2+}$ in the surface snow samples from coast to inland.

Site	Cl^-/Na^+	$nssSO_4^{2-}/SO_4^{2-}$	$MSA/nssSO_4^{2-}$	$nssCa^{2+}/Ca^{2+}$
	(W/W)	(%)	(W/W)	(%)
LH9601	1.07	−178	−0.01	−101
LHA006	1.12	6	5.53	−91
L156	0.98	29	1.09	−203
LH404	1.23	85	0.49	27
LH397	1.58	90	0.36	93
LH386	1.39	92	0.43	92
LGB72	1.42	93	0.34	55
LT987	1.83	95	0.28	89
LT981	2.19	97	0.23	89
LT976	1.63	96	0.25	90
LT971	2.57	95	0.28	92
LT966	1.69	94	0.36	76
LT961	1.99	96	0.38	63
LT956	1.84	95	0.46	57
LT951	1.76	97	0.32	89
LT946	2.24	97	0.41	89
LT941	1.80	97	0.25	79

The spatial distributions of sea-salt ions in the two snow pits were also analyzed. The concentrations of Cl^-, Na^+, and Mg^{2+} of the LHA006 snow pit ranged from 262.10 to 2660.70, 182.40 to 2205.96, and 27.66 to 223.38 μg L^{-1}, respectively, whereas those of the LGB69 snow pit ranged from 5.90 to 268.10, 2.02 to 195.51, and 0.53 to 28.75 μg L^{-1}, respectively (Table 6). Given that LHA006 is located in the steep coastal escarpment region, the mean concentrations of these three sea-salt ions were considerably higher at LHA006 than at LGB69, which can be attributed to the preferential wet or dry deposition of sea-salt aerosols.

Table 6. Mean, maximum, minimum, and standard deviation (σ) of major ion concentrations in the LHA006 and LGB69 snow pits.

Site	LHA006				LGB69			
	Mean	Maximum	Minimum	σ	Mean	Maximum	Minimum	σ
				(μg L^{-1})				
MSA	48.68	345.86	1.36	64.93	6.42	18.08	0.00	4.57
Cl^-	1046.18	2660.70	262.10	716.06	66.47	268.10	5.90	51.22
SO_4^{2-}	258.18	1126.74	121.17	170.50	38.80	104.08	11.85	20.84
$nssSO_4^{2-}$	35.19	580.68	−301.69	140.25	29.44	96.27	2.24	20.26
Na^+	883.13	2205.96	182.40	585.12	37.08	195.51	2.02	34.24
Mg^{2+}	93.07	223.38	27.66	58.51	7.25	28.75	0.53	6.01
$Ca2^+$	32.10	110.00	8.87	21.58	11.49	101.53	2.13	14.26
$nssCa^{2+}$	−1.46	87.11	−23.79	17.20	10.08	100.97	0.52	14.32

The snow pit results showed a clear difference in the mean Cl^-/Na^+ ratios between LHA006 (1.18) and LGB69 (1.79). As with the Cl^-/Na^+ ratio in the surface snow sample at LHA006, the mean Cl^-/Na^+ ratio of the LHA006 snow pit samples was also low and lower than that of the LGB69 snow pit samples. Thus, the low mean Cl^-/Na^+ ratio of the

LHA006 snow pit samples may also be related to the increased Na^+ concentrations driven by the steep slopes of the coastal escarpment.

3.1.2. Non-Sea-Salt Ions

The mass concentrations of $nssSO_4^{2-}$ and $nssCa^{2+}$ were calculated using the following equations and Na^+ was considered to be only provided by sea water:

$$nssSO_4^{2-} = SO_4^{2-} - Na^+ \times 0.2525, \quad (1)$$

$$nssCa^{2+} = Ca^{2+} - Na^+ \times 0.038, \quad (2)$$

where 0.2525 and 0.038 are the mass concentration ratios of $(SO_4^{2-})/(Na^+)$ and $(Ca^{2+})/(Na^+)$ in sea water, respectively [44–46].

The MSA concentrations showed an overall decreasing trend with increasing distance from the coast and/or altitude. High MSA concentrations obtained between 7.4 and 68 km (285–1041 m altitude) ranged between 2.77 and 145.82 μg L^{-1}. However, the data from the interior region (78–170 km or 1157–1852 m altitude) showed relatively low MSA concentrations (ranged from 17.60 to 48.09 μg L^{-1}) (Figure 5). The detailed MSA concentrations of the surface snow samples along the transect are shown in Table 3. The MSA concentrations showed a significant relationship with distance from the coast or altitude (Table 4). This implies that distance from the coast and/or altitude are the main factors that affect the spatial distribution of MSA.

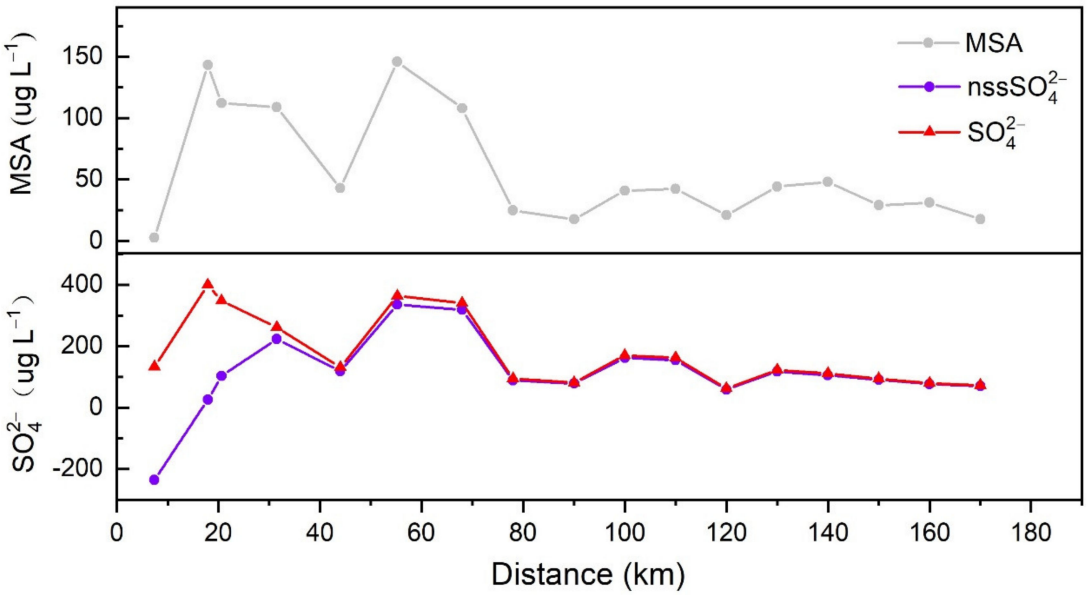

Figure 5. Concentration variations of MSA, $nssSO_4^{2-}$, and SO_4^{2-} with increasing distance from the coast.

The variation of $nssSO_4^{2-}$ concentrations was similar to that of the MSA concentrations (Figure 5). However, a few surface snow samples with negative and low $nssSO_4^{2-}/SO_4^{2-}$ percentages were observed in the steep coastal escarpment region within 20.6 km (Table 5), as discussed later. The $nssSO_4^{2-}$ concentrations showed high values (ranged from 118.45 to 335.38 μg L^{-1}) between 31.5 and 68 km (737–1041 m altitude). The relatively low $nssSO_4^{2-}$ concentrations (ranged from 58.48 to 162.24 μg L^{-1}) were obtained from 78 to 170 km (1157–1852 m altitude) (Figure 5). Table 3 shows the detailed $nssSO_4^{2-}$ concentrations of the surface snow samples along the transect. When the surface snow samples with negative and low $nssSO_4^{2-}/SO_4^{2-}$ percentages within 20.6 km were excluded, the $nssSO_4^{2-}$ concentrations exhibited a significant negative correlation with distance from the coast ($R = -0.624$, $p < 0.05$) or altitude ($R = -0.642$, $p < 0.05$), implying that the variation of $nssSO_4^{2-}$ is dependent both on distance from the coast and/or altitude. Moreover, the

high concentrations of MSA and nssSO_4^{2-} occurred between 7.4 and 68 km, whereas those of sea-salt ions appeared only between 7.4 and 20.6 km. This is because super-micrometric sea-salt aerosol particles have relatively shorter atmospheric residence times and undergo more efficient atmospheric scavenging process than sub-micrometric MSA and nssSO_4^{2-} aerosol particles in the coastal regions [5,47,48]. The nssSO_4^{2-} concentrations exhibited a significant correlation with MSA concentration (Table 4), which suggests that both of them are from the atmospheric oxidation of DMS, which is produced by phytoplankton activity in the ocean.

In general, nssSO_4^{2-} contributes mostly to the sulfate budget [27,30]. However, in the present study, the spatial distribution pattern of nssSO_4^{2-}/SO_4^{2-} ratios was characterized by their gradual increase and stabilization from the coast inland, and a few negative and low ratios of nssSO_4^{2-}/SO_4^{2-} were observed in the steep coastal escarpment region within 20.6 km (Table 5). Two main mechanisms have been proposed for the negative and low nssSO_4^{2-}/SO_4^{2-} percentages in coastal Antarctica. First, negative and low nssSO_4^{2-}/SO_4^{2-} percentages have been speculated to both originate from the underestimation of nssSO_4^{2-}. This implies that their sea-salt ions are likely from fractionated sea-salt aerosols produced by salty frost flowers on the sea ice surface at coastal Antarctica sites [2,19,49–51]. The SO_4^{2-}/Na^+ ratio of salty frost flowers is lower than that of sea water owing to the brine fractionation processes on the sea ice surface, which occur when the ice temperature decreases. Mirabilite ($Na_2SO_4 \cdot 10\ H_2O$) begins to precipitate at −8 °C but NaCl precipitation only begins at −26 °C. Thus, the use of original SO_4^{2-}/Na^+ ratio from sea water in the nssSO_4^{2-} calculations may cause the negative and low concentrations of nssSO_4^{2-} in the snow samples. The low nssSO_4^{2-}/SO_4^{2-} percentages can also be attributed to the atmospheric scavenging of sea-salt aerosol particles by wet and dry removal processes. Super-micrometric ssSO_4^{2-} aerosol particles have relatively shorter atmospheric residence times and undergo more efficient atmospheric scavenging process than sub-micrometric biogenic nssSO_4^{2-} aerosol particles in the coastal regions [5,47,48].

In the present study, it is unlikely that the effects of salty frost flower fractionation can be used to explain the negative and low nssSO_4^{2-}/SO_4^{2-} percentages that occurred only in the steep coastal escarpment region within 20.6 km. Given that the nssSO_4^{2-} calculation was based on Na^+, the increase of Na^+ concentrations driven by the steep slopes can affect the nssSO_4^{2-} calculations, resulting in negative or low nssSO_4^{2-} concentrations. Therefore, the negative and low nssSO_4^{2-}/SO_4^{2-} percentages in the steep coastal escarpment region within 20.6 km can be attributed to the increased Na^+ concentrations driven by the steep slopes of the coastal escarpment and the effects of atmospheric scavenging processes.

An inverse relationship has been reported between site temperature and MSA/nssSO_4^{2-} ratios in the marine atmospheric boundary layer of the southern hemisphere [52]. Higher MSA/nssSO_4^{2-} ratios (0.15–0.93, W/W) in the marine atmospheric boundary layer in summer were observed near coastal Antarctica, whereas lower MSA/nssSO_4^{2-} ratios (0.0024–0.12, W/W) were observed at mid and low latitudes [53]. Thus, the MSA/nssSO_4^{2-} ratios in snow samples from Antarctica can be used as a tracer of the latitudes of marine source regions of MSA and nssSO_4^{2-} at a given location, i.e., high MSA/nssSO_4^{2-} ratios in snow samples suggest that they are from a high-latitude marine source [54].

In the present study, a few abnormally negative and high MSA/nssSO_4^{2-} ratios were observed in the steep coastal escarpment region within 20.6 km. A negative MSA/nssSO_4^{2-} ratio (−0.01) was recorded at the LH9601 site at 7.4 km (285 m altitude). The highest MSA/nssSO_4^{2-} ratio (5.53) was recorded at the LHA006 site at 17.9 km (520 m altitude), followed by 1.09 at the L156 site at 20.6 km (586 m altitude) (Figure 6 and Table 5). As mentioned previously, the increased Na^+ concentrations driven by the steep slopes of the coastal escarpment can result in negative and low nssSO_4^{2-} concentrations. Consequently, abnormally negative and high MSA/nssSO_4^{2-} ratios occurred in the steep coastal escarpment region within 20.6 km. When the abnormally negative and high MSA/nssSO_4^{2-} ratios within 20.6 km were removed, the mean MSA/nssSO_4^{2-} value of the surface snow samples from Zhongshan Station to LGB69 was 0.34 ± 0.08 (Figure 6), which was in agree-

ment with the MSA/nssSO_4^{2-} ratios observed in the marine atmospheric boundary layer near coastal Antarctica, implying that the source regions of the MSA and nssSO_4^{2-} from Zhongshan Station to LGB69 are likely coastal sea areas.

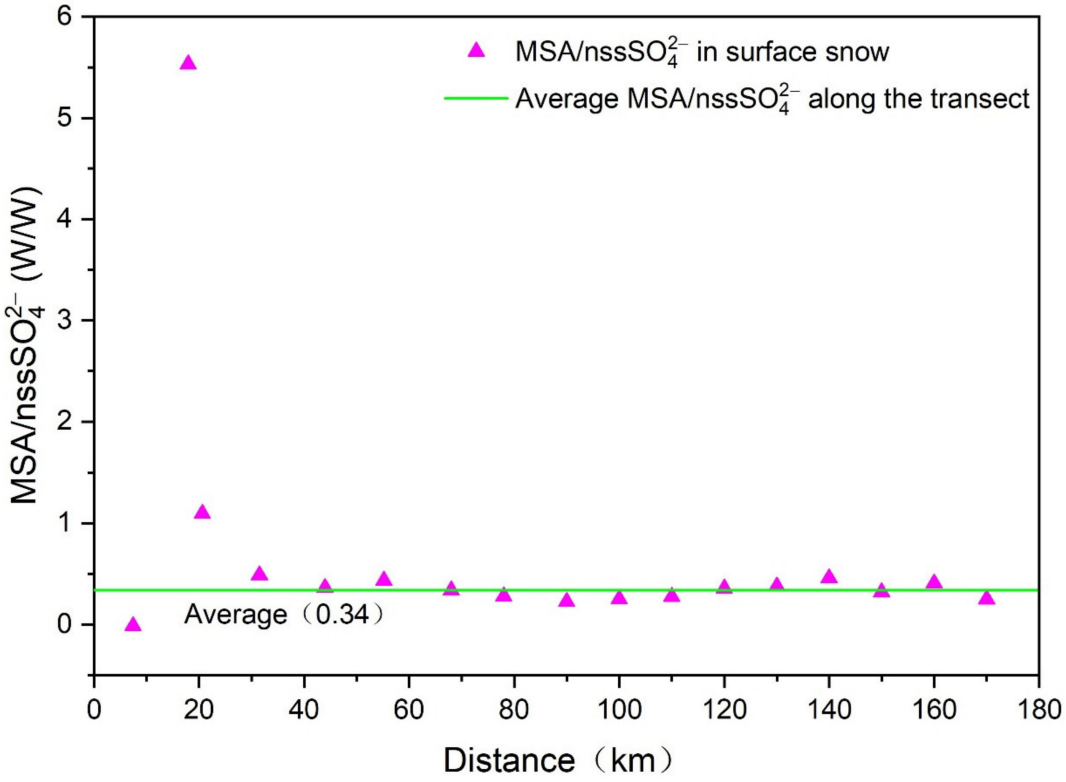

Figure 6. Variation of MSA/nssSO_4^{2-} ratios in the surface snow samples from coast to inland.

Ca^{2+} concentrations also showed an overall decreasing trend with increasing distance from the coast and/or altitude. High Ca^{2+} concentrations (ranged from 7.85 to 53.40 μg L^{-1}) were measured between 7.4 and 55.2 km (285–955 m altitude). However, the data from the interior region between 68 and 170 km (1041–1852 m altitude) exhibited relatively low Ca^{2+} concentrations (ranged from 1.44 to 14.76 μg L^{-1}) (Figure 7). The detailed Ca^{2+} concentrations of the surface snow samples along the transect are shown in Table 3. The Ca^{2+} concentrations showed a significant correlation with distance from the coast or altitude (Table 4), implying that the spatial distribution of Ca^{2+} from Zhongshan Station to LGB69 is also mainly affected by distance from the coast and/or altitude.

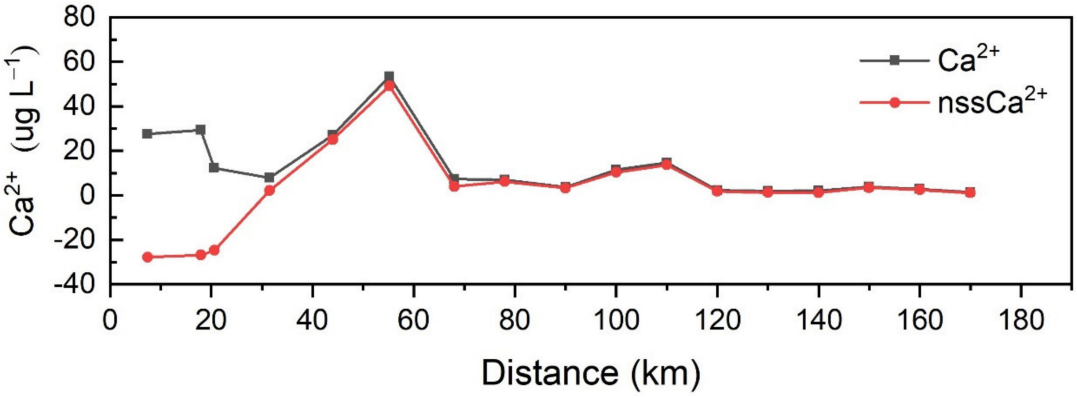

Figure 7. Concentration variations of Ca^{2+} and nssCa^{2+} with increasing distance from the coast.

The main sources of Ca^{2+} in Antarctic snow are continental dust and sea spray [55]. In the present study, the calculated $nssCa^{2+}/Ca^{2+}$ percentages in the surface snow samples from Zhongshan Station to LGB69 (Table 5) suggest that continental dust is the primary source for Ca^{2+} and the contribution from sea spray is relatively minor. However, similar to $nssSO_4^{2-}$, negative $nssCa^{2+}$ concentrations were also observed in the steep coastal escarpment region within 20.6 km (Table 3), which may also be because of the increased Na^+ concentrations driven by the steep slopes of the coastal escarpment.

The spatial distributions of non-sea-salt ions in the two snow pits were also simultaneously analyzed. The concentrations of $nssSO_4^{2-}$ and MSA of the LHA006 snow pit ranged from −301.69 to 580.68 and 1.36 to 345.86 μg L^{-1}, respectively, and those of the LGB69 snow pit ranged from 2.24 to 96.27 and 0 to 18.08 μg L^{-1}, respectively (Table 6). However, the mean $nssSO_4^{2-}/SO_4^{2-}$ percentage in the LHA006 snow pit (14%) was substantially lower than the LGB69 snow pit value (76%), which was similar to that at Hercules Névé (75%) [5] and lower than that at Talos Dome (88%) [4]. Moreover, the mean $MSA/nssSO_4^{2-}$ ratio in the LHA006 snow pit (1.38) was considerably higher than that of the LGB69 snow pit (0.22). These large differences in the mean $nssSO_4^{2-}/SO_4^{2-}$ percentage and mean $MSA/nssSO_4^{2-}$ ratio between the LHA006 and LGB69 snow pits can be explained by the increased Na^+ concentrations driven by the steep slopes of the coastal escarpment and effects of atmospheric scavenging processes.

The concentrations of Ca^{2+} of the LHA006 snow pit ranged from 8.87 to 110.00 μg L^{-1}, whereas those of the LGB69 snow pit ranged from 2.13 to 101.53 μg L^{-1} (Table 6). However, the calculated mean concentration of $nssCa^{2+}$ showed a negative value (−1.46 ± 17.20 μg L^{-1}) in the LHA006 snow pit samples (Table 6). As with the negative $nssCa^{2+}$ concentration in the surface snow sample at LHA006, the negative mean concentration of $nssCa^{2+}$ in the LHA006 snow pit samples can also be attributed to the increased Na^+ concentrations driven by the steep slopes of the coastal escarpment. The mean $nssCa^{2+}/Ca^{2+}$ percentage of the LGB69 snow pit samples (88%) shows that the $nssCa^{2+}$ contributes mostly to the total Ca^{2+}.

3.2. Spatial Variability of Isotopic Compositions

The spatial distributions of δD, $\delta^{18}O$, and d-excess from in the surface snow samples were analyzed. The second-order parameter d-excess was calculated following [56]:

$$\text{d-excess} = \delta D - 8 \times \delta^{18}O, \quad (3)$$

Both the δD and $\delta^{18}O$ values in the surface snow samples decreased with increasing distance from the coast and/or altitude (Figure 8), exhibiting significant negative correlations (Table 7). The detailed δD and $\delta^{18}O$ values in the surface snow samples along the transect are shown in Table 3. The lapse rates of δD and $\delta^{18}O$ with distance from the coast were respectively −54.17‰/100 km and −6.84‰/100 km (Table 8). The topographic features were revealed by the contour lines in Figure 1 and showed that the slope from Zhongshan Station to LGB69 was steeper than that between LGB69 and Dome A, causing the rapid decreases of δD and $\delta^{18}O$ values. The lapse rates of δD and $\delta^{18}O$ with distance from the coast along the transect from Zhongshan Station to LGB69 were therefore considerably larger than those along the transect from Zhongshan Station to Dome A. The lapse rates of δD and $\delta^{18}O$ with altitude from Zhongshan Station to LGB69 were respectively −5.99‰/100 m and −0.75‰/100 m, and lower than those from Zhongshan Station to Dome A (Table 8). This can still be attributed to the topographic difference between the transect from Zhongshan Station to LGB69 and that from LGB69 to Dome A.

The relationship between δD and $\delta^{18}O$ values in the surface snow samples is given as

$$\delta D = (7.90 \pm 0.17)\ \delta^{18}O - (0.09 \pm 3.33)\ (R^2 = 0.99, n = 17), \quad (4)$$

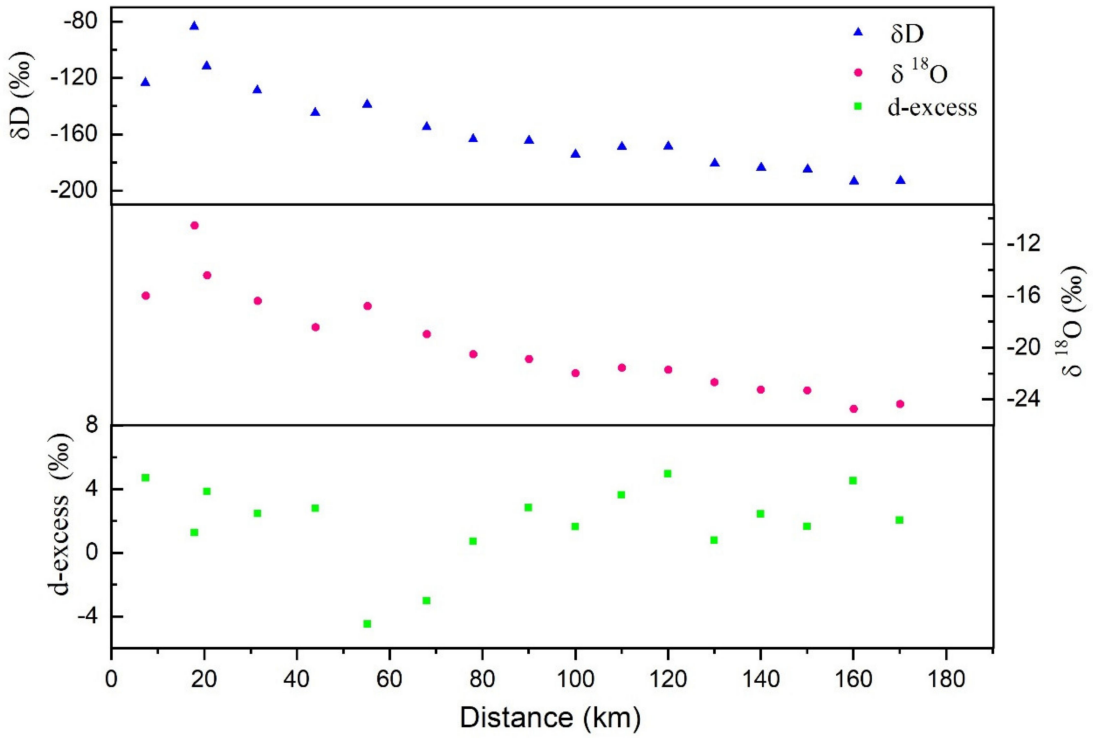

Figure 8. Variations of δD, $\delta^{18}O$, and d-excess of the surface snow samples as a function of distance from the coast.

Table 7. Correlation matrix of the stable isotope values of the surface snow samples along with distance from the coast and altitude.

	δD	$\delta^{18}O$	d-Excess	Distance	Altitude
δD	1	0.997 *	−0.077	−0.929 *	−0.933 *
$\delta^{18}O$		1	−0.157	−0.929 *	−0.929 *
d-excess			1	0.111	0.064
Distance				1	0.991 *
Altitude					1

* The data are significantly correlated at $p < 0.01$.

Table 8. Gradients of the stable isotope values with distance from the coast and altitude along the transect from Zhongshan Station to LGB69 or to Dome A.

	This Study	Li et al. [27]	Xiao et al. [26]
transect	Zhongshan Station-LGB69	Zhongshan Station-Dome A	Zhongshan Station-Dome A
date	2001/2002	2012/2013	2007/2008
δD-distance	−54.17‰/100 km	−18.15‰/100 km	−16.3‰/100 km
δD-altitude	−5.99‰/100 m	−7.14‰/100 m	−8.5‰/100 m
$\delta^{18}O$-distance	−6.84‰/100 km	−2.37‰/100 km	−2.20‰/100 km
$\delta^{18}O$- altitude	−0.75‰/100 m	−0.93‰/100 m	−1.1‰/100 m
d-excess-distance	0.53‰/100 km	-	1.31‰/100 km
d-excess-altitude	0.03‰/100 m	-	0.6‰/100 m
d-excess variation range	−4.47‰–4.97‰	−3.38‰–15.12‰	2.47‰–39.74‰

The slope between δD and $\delta^{18}O$ was 7.90 ± 0.17 and lower than that of GMWL, but higher than the values reported by Li et al. (7.78 ± 0.04) [27] and Xiao et al. (7.50 ± 0.1) [26]. This indicates that more intense kinetic fractionation processes occur during snow formation in the inland between LGB69 and Dome A

The d-excess values did not show a significant relationship with distance from the coast (R = 0.111, p = 0.67) or altitude (R = 0.064, p = 0.80) (Table 7), indicating that the spatial distribution of d-excess from Zhongshan Station to LGB69 is mainly affected by the moisture source region. The gradients of d-excess with distance from the coast and altitude were 0.53‰/100 km and 0.03‰/100 m, respectively, which were substantially lower than values reported by Xiao et al. [26] (Table 8). The d-excess varied from −4.47‰ to 4.97‰ (Table 8), a considerably smaller range than those reported by Li et al. [27] and Xiao et al. [26], from Zhongshan Station to Dome A. The variation of d-excess was stable, which suggests that the transect from Zhongshan Station to LGB69 has the same moisture source region.

The mean values of δD, $\delta^{18}O$, and d-excess in the snow pit samples were simultaneously analyzed. The δD and $\delta^{18}O$ values at LHA006 ranged from −178.19 to −121.15‰ and −23.26 to −15.04‰, respectively, whereas those at LGB69 ranged from −302.09 to −200.27‰ and −37.96 to −25.04‰, respectively (Table 9). The d-excess values at LHA006 ranged between −1.25 and 10.88‰ with a mean value of 3.32 ± 2.53‰. The d-excess values at LGB69 ranged between −6.64 and 9.33‰ with a mean value of 2.56 ± 3.59‰ (Table 9). Previous studies noted that the d-excess values in Antarctica are low (~5‰) and stable below 2000 m altitude, which implies that the moisture source regions are coastal sea areas [32,57]. In our study, the altitudes of both LHA006 and LGB69 are below 2000 m. Furthermore, the mean d-excess values in the LHA006 and LGB69 snow pits were low and similar, indicating that the precipitation at both LHA006 and LGB69 originates from the same moisture source region (i.e., coastal sea area).

Table 9. Mean, maximum, minimum, and standard deviation (σ) of δD, $\delta^{18}O$, and d-excess values in the LHA006 and LGB69 snow pits.

Site	LHA006				LGB69			
	Mean	Maximum	Minimum	σ	Mean	Maximum	Minimum	σ
				(‰)				
δD	−143.36	−121.15	−178.19	16.47	−244.71	−200.27	−302.09	27.22
$\delta^{18}O$	−18.33	−15.04	−23.26	2.10	−30.91	−25.04	−37.96	3.22
d-excess	3.32	10.88	−1.25	2.53	2.56	9.33	−6.64	3.59
Sample number	49 *				89 *			

* One sample was lost from the LHA006 and LGB69 snow pits.

4. Conclusions

This study reports the spatial distribution patterns and sources of ions and stable isotopes as well as factors that influence the deposition of major ions and the composition of stable isotopes in surface snow and snow pit samples obtained along a transect from Zhongshan Station to LGB69, East Antarctica.

The spatial distributions of sea-salt ions (Cl^-, Na^+, and Mg^{2+}) along the transect showed that sea-salt ions exponentially decreased with increasing distance from the coast or altitude. The distance from the coast and/or altitude are the two major factors that influence the spatial distributions of sea-salt ions. High Cl^-, Na^+, and Mg^{2+} concentrations that occurred specifically in the steep coastal escarpment region within 20.6 km can be attributed to the preferential wet or dry deposition of sea-salt aerosols. The average Cl^-/Na^+ ratio of the surface snow samples from Zhongshan Station to LGB69 was 1.67 ± 0.44, which suggests that sea salt is the main source of Cl^- and Na^+ along the transect. However, the steep slopes of the coastal escarpment can result in wind redistribution-induced snow redistribution, leading to increased Na^+ concentrations. Thus, the Cl^-/Na^+ ratios, $nssSO_4^{2-}$, $MSA/nssSO_4^{2-}$ ratios, and $nssCa^{2+}$ values calculated based on Na^+ showed a few abnormal values in the steep coastal escarpment region within 20.6 km. MSA, $nssSO_4^{2-}$, and Ca^{2+} concentrations showed overall decreasing trends with increasing distance from the coast and/or altitude. The distance from the coast and/or altitude are the major

influencing factors of the spatial distributions of MSA, $nssSO_4^{2-}$, and Ca^{2+}. The similar spatial variation and significant correlation between MSA and $nssSO_4^{2-}$ in the surface snow indicate their common source, i.e., biogenic activity. When the abnormally negative and high MSA/$nssSO_4^{2-}$ ratios within 20.6 km were removed, the mean MSA/$nssSO_4^{2-}$ value of surface snow samples was 0.34 ± 0.08, which suggests that their source regions are likely coastal sea areas. The $nssCa^{2+}/Ca^{2+}$ percentages in the surface snow and LGB69 snow pit samples indicated that continental dust is the primary source for Ca^{2+} along the transect from Zhongshan Station to LGB69.

In addition, δD and $\delta^{18}O$ values decreased from the coast inland. Both δD and $\delta^{18}O$ in the surface snow exhibited significant negative correlations with distance from the coast and/or altitude. The lapse rates of δD and $\delta^{18}O$ from Zhongshan Station to LGB69 were larger than those from Zhongshan Station to Dome A because of the steeper slope of the former transect. The d-excess values did not show a significant relationship with distance from the coast or altitude, indicating that the moisture source region is the major factor that affected the spatial distribution of d-excess from Zhongshan Station to LGB69. The variation of d-excess in the surface snow samples was stable and the mean d-excess values in the LHA006 and LGB69 snow pits were low and similar (3.32 ± 2.53‰ and 2.56 ± 3.59‰, respectively), which indicates that the moisture source region between Zhongshan Station and LGB69 is the coastal sea area.

The glaciochemistry results of the surface snow and snow pit samples along the transect from Zhongshan Station to LGB69 suggest that the ionic and moisture source region is the coastal sea area, which will be useful for interpreting the temporal variability of chemical ions and isotopes from ice cores drilled in the coastal regions of Princess Elizabeth Land.

Author Contributions: Conceptualization, W.H. and M.Y.; Data curation, M.Y. and R.M.; Formal analysis, W.H., M.Y., L.L., C.A. and Y.Z.; Funding acquisition, M.Y. and Z.Q.; Investigation, M.Y. and C.X.; Methodology, W.H., M.Y. and R.M.; Project administration, M.Y.; Supervision, M.Y.; Validation, W.H., Z.Q., L.L., C.A. and Y.Z.; Writing—original draft, W.H.; Writing—review and editing, W.H. and M.Y. All authors have read and agreed to the published version of the manuscript.

Funding: This research was supported by the National Natural Science Foundation of China (41676192; 51676144).

Institutional Review Board Statement: Not applicable.

Informed Consent Statement: Not applicable.

Data Availability Statement: The data that support the findings of this study are available from the corresponding author, upon reasonable request.

Acknowledgments: We thank Susan Foord and Jack Triest of the British Antarctic Survey for their help with cutting of the ice cores, and Louise Gemma Thilthorpe of the British Antarctic Survey for assistance with ion chromatography analysis of snow and ice samples.

Conflicts of Interest: The authors declare no conflict of interest.

References

1. Delmas, R.J. Environmental information from ice cores. *Rev. Geophys.* **1992**, *30*, 1–21. [CrossRef]
2. Wolff, E.W.; Rankin, A.M.; Röthlisberger, R. An ice core indicator of Antarctic sea ice production? *Geophys. Res. Lett.* **2003**, *30*, 2158. [CrossRef]
3. Abram, N.J.; Mulvaney, R.; Wolff, E.W.; Mudelsee, M. Ice core records as sea ice proxies: An evaluation from the Weddell Searegion of Antarctica. *J. Geophys. Res. Atmos.* **2007**, *112*, D15101. [CrossRef]
4. Becagli, S.; Benassai, S.; Castellano, E.; Largiuni, O.; Migliori, A.; Traversi, R.; Flora, O.; Udisti, R. Chemical characterization of the last 250 years of snow deposition at Talos Dome (East Antarctica). *Int. J. Environ. Anal. Chem.* **2004**, *84*, 523–536. [CrossRef]
5. Traversi, R.; Becagli, S.; Castellano, E.; Largiuni, O.; Migliori, A.; Severi, M.; Frezzotti, M.; Udisti, R. Spatial and temporal distribution of environmental markers from Coastal to Plateau areas in Antarctica by firn core chemical analysis. *Int. J. Environ. Anal. Chem.* **2004**, *84*, 457–470. [CrossRef]

6. Saltzman, E.S. Ocean/Atmosphere Cycling of Dimethylsulfide. In *Ice Core Studies of Global Biogeochemical Cycles. NATO ASI Series (Series I: Global Environmental Change)*; Delmas, R.J., Ed.; Springer: Berlin/Heidelberg, Germany, 1995; Volume 30, pp. 65–89. [CrossRef]
7. Saigne, C.; Legrand, M. Measurements of methanesulphonic acid in Antarctic ice. *Nature* **1987**, *330*, 240–242. [CrossRef]
8. Legrand, M.; Feniet-Saigne, C. Methanesulfonic acid in south polar snow layers: A record of strong El Niño? *Geophys. Res. Lett.* **1991**, *18*, 187–190. [CrossRef]
9. Castebrunet, H.; Martinerie, P.; Genthon, C.; Cosme, E. A three-dimensional model study of methanesulphonic acid to non sea salt sulphate ratio at mid and high-southern latitudes. *Atmos. Chem. Phys. Atmos.* **2009**, *9*, 9449–9469. [CrossRef]
10. Cole-Dai, J.; Mosley-Thompson, E.; Wight, S.P.; Thompson, L.G. A 4100-year record of explosive volcanism from an East Antarctica ice core. *J. Geophys. Res. Atmos.* **2000**, *105*, 24431–24441. [CrossRef]
11. Ren, J.; Li, C.; Hou, S.; Xiao, C.; Qin, D.; Li, Y.; Ding, M. A 2680 year volcanic record from the DT-401 East Antarctic ice core. *J. Geophys. Res. Atmos.* **2010**, *115*, 11301. [CrossRef]
12. Hammer, C.U. Initial direct current in the buildup of space charges and the acidity of ice cores. *J. Phys. Chem.* **1983**, *87*, 4099–4103. [CrossRef]
13. Hammer, C.U. Acidity of polar ice cores in relation to absolute dating, past volcanism, and Radio-Echoes. *J. Glaciol.* **1980**, *25*, 359–372. [CrossRef]
14. Legrand, M.; Delmas, R.J. A 220-year continuous record of volcanic H_2SO_4 in the Antarctic ice sheet. *Nature* **1987**, *327*, 671–676. [CrossRef]
15. Masson-Delmotte, V.; Hou, S.; Ekaykin, A.; Jouzel, J.; Aristarain, A.; Bernardo, R.T.; Bromwich, D.; Cattani, O.; Delmotte, M.; Falourd, S.; et al. A Review of Antarctic Surface Snow Isotopic Composition: Observations, Atmospheric Circulation, and Isotopic Modeling*. *J. Clim.* **2008**, *21*, 3359–3387. [CrossRef]
16. Kurita, N. Origin of Arctic water vapor during the ice-growth season. *Geophys. Res. Lett.* **2011**, *38*, L02709. [CrossRef]
17. Wang, Y.; Sodemann, H.; Hou, S.; Masson-Delmotte, V.; Jouzel, J.; Pang, H. Snow accumulation and its moisture origin over Dome Argus, Antarctica. *Clim. Dyn.* **2013**, *40*, 731–742. [CrossRef]
18. Vance, T.R.; Roberts, J.L.; Moy, A.D.; Curran, M.A.J.; Tozer, C.R.; Gallant, A.J.E.; Abram, N.J.; van Ommen, T.D.; Young, D.A.; Grima, C.; et al. Optimal site selection for a high-resolution ice core record in East Antarctica. *Clim. Past* **2016**, *12*, 595–610. [CrossRef]
19. Vega, C.P.; Isaksson, E.; Schlosser, E.; Divine, D.; Martma, T.; Mulvaney, R.; Eichler, A.; Schwikowski-Gigar, M. Variability of sea salts in ice and firn cores from Fimbul Ice Shelf, Dronning Maud Land, Antarctica. *Cryosphere* **2018**, *12*, 1681–1697. [CrossRef]
20. Nyamgerel, Y.; Han, Y.; Kim, S.; Hong, S.-B.; Lee, J.; Hur, S.D. Chronological characteristics for snow accumulation on Styx Glacier in northern Victoria Land, Antarctica. *J. Glaciol.* **2020**. [CrossRef]
21. Kärkäs, E.; Teinilä, K.; Virkkula, A.; Aurela, M. Spatial variations of surface snow chemistry during two austral summers in western Dronning Maud Land, Antarctica. *Atmos. Environ.* **2005**, *39*, 1405–1416. [CrossRef]
22. Zhang, M.J.; Li, Z.Q.; Xiao, C.D.; Ren, J.W.; Qin, D.H.; Kang, J.C.; Li, J. Decreasing trend of temperature in Princess Elizabeth Land, Antarctica in the past 150 years. *Chin. Sci. Bull.* **2002**, *47*, 1474–1478. [CrossRef]
23. Hou, S.; Li, Y.; Xiao, C.; Pang, H.; Xu, J. Preliminary results of the close-off depth and the stable isotopic records along a 109.91 m ice core from Dome A, Antarctica. *Sci. China Ser. D Earth Sci.* **2009**, *52*, 1502–1509. [CrossRef]
24. Ding, M.; Xiao, C.; Jin, B.; Ren, J.; Qin, D.; Sun, W. Distribution of $\delta^{18}O$ in surface snow along a transect from Zhongshan Station to Dome A, East Antarctica. *Chin. Sci. Bull.* **2010**, *55*, 2709–2714. [CrossRef]
25. Ren, J.W.; Sun, J.Y.; Qin, D.H. Preliminary results of ionic concentrations in snow pits along the Zhongshan–Dome A traverse route, Antarctica. *Ann. Glaciol.* **2004**, *39*, 155–160. [CrossRef]
26. Xiao, C.; Ding, M.; Masson-Delmotte, V.; Zhang, R.; Jin, B.; Ren, J.; Li, C.; Werner, M.; Wang, Y.; Cui, X.; et al. Stable isotopes in surface snow along a traverse route from Zhongshan station to Dome A, East Antarctica. *Clim. Dyn.* **2013**, *41*, 2427–2438. [CrossRef]
27. Li, C.; Xiao, C.; Shi, G.; Ding, M.; Qin, D.; Ren, J. Spatial and temporal variability of marine-origin matter along a transect from Zhongshan Station to Dome A, Eastern Antarctica. *J. Environ. Sci.* **2016**, *46*, 190–202. [CrossRef]
28. Li, C.; Qin, X.; Ding, M.; Guo, R.; Xiao, C.; Hou, S.; Bian, L.; Qin, D.; Ren, J. Temporal variations in marine chemical concentrations in coastal areas of eastern Antarctica and associated climatic causes. *Quat. Int.* **2014**, *352*, 16–25. [CrossRef]
29. Mulvaney, R.; Wolff, E.W. Spatial variability of the major chemistry of the Antarctic ice sheet. *Ann. Glaciol.* **1994**, *20*, 440–447. [CrossRef]
30. Khodzher, T.V.; Golobokova, L.P.; Osipov, E.Y.; Shibaev, Y.A.; Lipenkov, V.Y.; Osipova, O.P.; Petit, J.R. Spatial-temporal dynamics of chemical composition of surface snow in East Antarctica along the Progress station-Vostok station transect. *Cryosphere* **2014**, *8*, 931–939. [CrossRef]
31. Minikin, A.; Wagenbach, D.; Graf, W.; Kipfstuhl, J. Spatial and seasonal variations of the snow chemistry at the central Filchner-Ronne Ice Shelf, Antarctica. *Ann. Glaciol.* **1994**, *20*, 283–290. [CrossRef]
32. Ren, J.W.; Qin, D.H. Distribution of deuterium excess in surface snow of the Antarctic ice sheet. *Chin. Sci. Bull.* **1995**, *40*, 1629–1633.
33. Ding, M.; Xiao, C.; Li, Y.; Ren, J.; Hou, S.; Jin, B.; Sun, B. Spatial variability of surface mass balance along a traverse route from Zhongshan station to Dome A, Antarctica. *J. Glaciol.* **2011**, *57*, 658–666. [CrossRef]

34. Li, R.; Xiao, C.; Sneed, S.; Yan, M. A continuous 293-year record of volcanic events in an ice core from Lambert Glacier basin, East Antarctica. *Antarct. Sci.* **2012**, *24*, 293–298. [CrossRef]
35. Lis, G.; Wassenaar, L.I.; Hendry, M.J. High-Precision Laser Spectroscopy D/H and $^{18}O/^{16}O$ Measurements of Microliter Natural Water Samples. *Anal. Chem.* **2008**, *80*, 287–293. [CrossRef] [PubMed]
36. Mahalinganathan, K.; Thamban, M.; Laluraj, C.M.; Redkar, B.L. Relation between surface topography and sea-salt snow chemistry from Princess Elizabeth Land, East Antarctica. *Cryosphere* **2012**, *6*, 505–515. [CrossRef]
37. Ma, Y.F.; Bian, L.G.; Xiao, C.D.; Allison, I.; Zhou, X.J. Near surface climate of the traverse route from Zhongshan Station to Dome A, East Antarctica. *Antarct. Sci.* **2010**, *22*, 443–459. [CrossRef]
38. Bintanja, R.; Severijns, C.; Haarsma, R.; Hazeleger, W. The future if Antarctica's surface wings simulated by a high-resolution global climate model: 1. Model description and validation. *J. Geophys. Res. Atmos.* **2014**, *119*, 7136–7159. [CrossRef]
39. King, J.C.; Turner, J. *Antarctic Meteorology and Climatology*; Cambridge University Press (CUP): Cambridge, UK, 1997.
40. Suzuki, T.; Iizuka, Y.; Matsuoka, K.; Furukawa, T.; Kamiyama, K.; Watanabe, O. Distribution of sea salt components in snow cover along the traverse route from the coast to Dome Fuji station 1000 km inland at east Dronning Maud Land, Antarctica. *Tellus B* **2002**, *54*, 407–411. [CrossRef]
41. Broecker, W.S.; Peng, T.H. Tracers in the sea. In *Lamont-Doherty Geological Observatory*; Eldigio Press: New York, NY, USA, 1982.
42. Röthlisberger, R.; Mulvaney, R.; Wolff, E.W.; Hutterli, M.A.; Bigler, M.; De Angelis, M.; Hansson, M.E.; Steffensen, J.P.; Udisti, R. Limited dechlorination of sea-salt aerosols during the last glacial period: Evidence from the European Project for Ice Coring in Antarctica (EPICA) Dome C ice core. *J. Geophys. Res. Atmos.* **2003**, *108*, 4526. [CrossRef]
43. Frezzotti, M.; Gandolfi, S.; Urbini, S. Snow megadunes in Antarctica: Sedimentary structure and genesis. *J. Geophys. Res. Atmos.* **2002**, *107*, ACL 1-1. [CrossRef]
44. Holland, H.D. *The Chemistry of the Atmosphere and Oceans*; Wiley: New York, NY, USA, 1978; p. 351.
45. De Angelis, M.; Steffensen, J.P.; Legrand, M.; Clausen, H.; Hammer, C. Primary aerosol (sea salt and soil dust) deposited in Greenland ice during the last climatic cycle: Comparison with east Antarctic records. *J. Geophys. Res. Oceans* **1997**, *102*, 26681–26698. [CrossRef]
46. Summerhayes, C.P.; Thorpe, S.A. *Oceanography: An Illustrated Guide*; Wiley: New York, NY, USA, 1996; Chapter 11; pp. 165–181.
47. Becagli, S.; Proposito, M.; Benassai, S.; Gragnani, R.; Magand, O.; Traversi, R.; Udisti, R. Spatial distribution of biogenic sulphur compounds (MSA, $nssSO_4^{2-}$) in the northern Victoria Land–Dome C–Wilkes Land area, East Antarctica. *Ann. Glaciol.* **2005**, *41*, 23–31. [CrossRef]
48. Benassai, S.; Becagli, S.; Gragnani, R.; Magand, O.; Proposito, M.; Fattori, I.; Traversi, R.; Udisti, R. Sea-spray deposition in Antarctic coastal and plateau areas from ITASE traverses. *Ann. Glaciol.* **2005**, *41*, 32–40. [CrossRef]
49. Rankin, A.M.; Auld, V.; Wolff, E.W. Frost flowers as a source of fractionated sea salt aerosol in the polar regions. *Geophys. Res. Lett.* **2000**, *27*, 3469–3472. [CrossRef]
50. Rankin, A.M.; Wolff, E.W.; Martin, S. Frost flowers: Implications for tropospheric chemistry and ice core interpretation. *J. Geophys. Res. Atmos.* **2002**, *107*, AAC-4. [CrossRef]
51. Abram, N.J.; Wolff, E.W.; Curran, M.A.J. A review of sea ice proxy information from polar ice cores. *Quat. Sci. Rev.* **2013**, *79*, 168–183. [CrossRef]
52. Bates, T.S.; Calhoun, J.A.; Quinn, P.K. Variations in the Methanesulphonate to Sulphate Molar Ratio in Submicrometer Marine Aerosol Particles over the South Pacific Ocean. *J. Geophys. Res. Atmos.* **1992**, *97*, 9859–9865. [CrossRef]
53. Chen, L.; Wang, J.; Gao, Y.; Xu, G.; Yang, X.; Lin, Q.; Zhang, Y. Latitudinal distributions of atmospheric MSA and MSA/nss-SO_4^{2-} ratios in summer over the high latitude regions of the Southern and Northern Hemispheres. *J. Geophys. Res. Atmos.* **2012**, *117*. [CrossRef]
54. Legrand, M.; Feniet-Saigne, C.; Saltzman, E.S.; Germain, C. Spatial and temporal variations of methanesulfonic acid and non sea salt sulfate in Antarctic ice. *J. Atmos. Chem.* **1992**, *14*, 245–260. [CrossRef]
55. Legrand, M.; Mayewski, P. Glaciochemistry of polar ice cores: A review. *Rev. Geophys.* **1997**, *35*, 219–243. [CrossRef]
56. Dansgaard, W. Stable isotopes in precipitation. *Tellus* **1964**, *16*, 436–468. [CrossRef]
57. Petit, J.R.; White, J.W.C.; Young, N.W.; Jouzel, J.; Korotkevich, Y.S. Deuterium excess in recent Antarctic snow. *J. Geophys. Res. Atmos.* **1991**, *96*, 5113–5122. [CrossRef]